Numerical modeling of elastic waves propagation in isotropic vertically inhomogeneous media.

Sitamai W. Ajiduah, Gary F. Margrave and P. F. Daley

SUMMARY

A method for calculation of complete theoretical seismograms for coupled P-Sv wave propagation in a vertically inhomogeneous media has been studied. Called the AMM method (for Alekseev-Mikhailenko), it is based on a combination of partial separation of variables via a finite Hankel transform over lateral coordinates and finite-differencing in time and depth. Results of theoretical seismograms for an isotropic vertically inhomogeneous model are presented in this paper and the effects of incidence angle and free-surface on component amplitudes are also investigated. Amplitudes from the AMM computations are compared with computations from the exact Zoeppritz equations for angles up to 60 degrees. All the computed amplitudes from AMM methods matched Zoeppritz amplitude at near vertical incidence up to 10 degrees (0.5km source-receiver offset). The P-P AMM and the P-P Zoeppritz amplitudes have the same trend for all pre-critical and post-critical angles; at the critical angle, Zoeppritz predicts an abrupt rise in amplitude while the AMM amplitudes show a gradual rise with a maximum beyond critical angle. The P-S amplitudes predicted from Zoeppritz matched with P-S AMM amplitudes only at near offset.

INTRODUCTION

Synthetic seismograms have been used routinely in the interpretation of seismic data and as key ingredients in anisotropic modelling and waveform inversion. Many different techniques now exist that can be used to calculate theoretical seismograms. The computation of synthetic seismograms basically involves: the transformation of a hyperbolic partial-differential wave equation into an ordinary differential equation, the solution of this ordinary differential equation with the appropriate radiation and boundary conditions, and the evaluation of the inverse transforms. However, difficulties arise for realistic anisotropy and/or anelasticity models and to be useful, calculations must be efficient. To obtain a more efficient calculation we will employ the Alekseev-Mikhailenko method (referred to as AMM in this paper). This method combines a finite integral transform over the lateral spatial co-ordinates and finite-difference method in time and depth so as to reduce the dimensionality of the wave propagation problem. Previous and detailed work on this method can be found in Martynov and Mikhailenko (1979), Alekseev & Mikhailenko (1980), and Daley, et.al. (2008, 2012) and CREWES volumes. Many reports by P. F. Daley in the recent CREWES volumes compile insightful discussions on this methods in details as well as its practical implementation. This method is as fast as most finite-difference programs in two spatial variables and time, with the benefit that grid dispersion may be almost entirely eliminated (to within 2 or 3%) (Pascoe et.al., 1988) by utilizing a band-limited source pulse and establishing the number of terms to adequately approximate the infinite series that comprises the inverse finite integral transform (In addition, out-of-plane spreading is included, which is not the case for a pure finite-difference scheme in two spatial variables and time. The compute time of the AMM method

unlike the reflectivity method (Muller, 1985) is independent of the number of layer. This is an added advantage of using the AMM method.

Our goal here is to present a brief review of this method and to compare the results with ray theory and amplitudes from plane-waves Zoeppritz equation after correction for geometric spreading, wavelet effect and receiver-emergence angle effect. Surface conversion effects, also called the free-surface effect, at the free-surface will also be investigated.

THEORY

Details of the AMM method used here follow after the compiled reports and publications of Daley's papers. The equation of motion for a coupled P-Sv wave propagating in a radially symmetric, vertically inhomogeneous medium can be written below; for the radial component (eqn. 1) and vertical component of displacement wavefield (eqn.2) of an explosive point source F.

$$\rho \frac{\partial^2 U}{\partial t^2} = c_{11}\left[\frac{\partial^2 U}{\partial r^2} + \frac{1}{r}\frac{\partial U}{\partial r} - \frac{U}{r}\right] + c_{13}\frac{\partial^2 U}{\partial r \partial z} + \frac{\partial}{\partial z}\left[c_{55}\left(\frac{\partial U}{\partial z} + \frac{\partial V}{\partial r}\right)\right] + \rho F_r, \quad (1)$$

$$\rho \frac{\partial^2 V}{\partial t^2} = c_{55}\left[\frac{\partial}{\partial r}\left(\frac{\partial U}{\partial z} + \frac{\partial V}{\partial r}\right) + \frac{1}{r}\left(\frac{\partial U}{\partial z} + \frac{\partial V}{\partial r}\right)\right] + \frac{\partial}{\partial z}\left[c_{13}\left(\frac{\partial U}{\partial r} + \frac{U}{r}\right)\right] + \rho F_z, \quad (2)$$

with the normal stress and tangential stress set to zero at the free surface - free surface boundary conditions; the initial values for displacement and velocity at time, $t = 0 \; and \; for \; r, z > 0$ is set to zero (initial conditions); $U(r,z,t) \; and \; V(r,z,t)$ are the radial and vertical component of the particle displacement vector $\boldsymbol{u} \equiv \boldsymbol{u}(r,z,t) = (U(r,z,t), V(r,z,t))$. The azimuthal component equals zero due to radial symmetry. The Voigt notation for stiffness parameter is c_{ij} , $F_r \; and \; F_z$ are the components of the explosive point source force vector describing the action of the source in time and space. The source wavelet is a Gabor wavelet, defined in time domain as $f(t) = \cos(2\pi f_0 t) \exp\left[-\left(\frac{2\pi f_0 t}{\gamma}\right)^2\right]$, where f_0 is the dominant frequency of the source wavelet and the dimensionless quantity γ (γ = 4 to 5) is a measure of the width of the Gaussian term and controls the side lobes in the time domain.

The purpose of using AMM is to reduce the spatial dimensionality of the problem by introducing finite Hankel transforms given below in equation 3 and 4. The finite Hankel transform consists of an integration over a finite range of r, say $0 < r < a$, where 'a' is a pseudo-boundary suitably chosen so that no spurious reflections from this lateral perfectly reflecting boundary are present in the synthetic traces in the space - time region being considered. It also eliminates terms in the finite transform of derivatives that appear when integrating by parts. The particle displacement vector $\boldsymbol{u}(r,z,t)$ can be written in the transformed domain as $\boldsymbol{G}(k_i,z,t) = (S(k_i,z,t), R(k_i,z,t))$ where

$$S(k_i,z,t) = \int_0^a U(r,z,t)\, J_i(k_i r) r dr, \quad (3)$$

$$R(\widetilde{k_i},z,t) = \int_0^a V(r,z,t)\, J_0(\widetilde{k_i} r) r dr, \quad (4)$$

k_i and $\widetilde{k_i}$, are the roots of the transcendental equations $J_i(k_i r) = 0$ and $J_0(\widetilde{k_i} r) = 0$ respectively. The choice of the order of Hankel integral transform to be applied is determined by the form of the pair of partial differential equations that describe the motion of the medium subjected to a body force. The transforms appropriate to the boundary-value problem of 1 and 2 with boundary and initial conditions. A finite first-order Hankel transform is applied to $U(r,z,t)$ and τ_{rz}, and a finite zero-order transform is applied to $V(r,z,t)$ and σ_{zz}, (Alekseev and Mikhailenko 1980, Aki and Richards 1980). The finite inverse transform pair for 3 and 4 are given by

$$U(r,z,t) = \frac{2}{a^2}\sum_{i=1}^{\infty} \frac{S(k_i,z,t)J_i(k_i r)}{[J_2(k_i r)]^2} \quad , \tag{5}$$

$$V(r,z,t) = \frac{2}{a^2}\sum_{i=1}^{\infty} \frac{R(k_i,z,t)J_0(k_i r)}{[J_0(k_i r)]^2}, \tag{6}$$

where - $J_2(k_i a) = J_0(k_i a) - \frac{2}{k_i a} J_1(k_i r)$ has been used but not derived here. Both the inverse series summations can be taken over the roots of one rather than two transcendental equations and as a consequence, the transformed vector field $\boldsymbol{G}(r,z,t) = (S(k_i,z,t), R(k_i,z,t))$. Upon application of the transforms given by 4 and 5 to the second-order hyperbolic PDE wave equation of 1 and 2 yield the following transformed wave equation and can be written as

$$\rho \frac{\partial^2 S}{\partial t^2} = \frac{\partial}{\partial z}\left[c_{55}\frac{\partial S}{\partial z} - k_i c_{55} R \right] + k_i c_{13}\frac{\partial R}{\partial z} - {k_i}^2 c_{11} S + \rho F_r, \tag{7}$$

$$\rho \frac{\partial^2 R}{\partial t^2} = \frac{\partial}{\partial z}\left[c_{33}\frac{\partial R}{\partial z} - k_i c_{13} S \right] + k_i c_{55}\frac{\partial S}{\partial z} - {k_i}^2 c_{55} R + \rho F_z, \tag{8}$$

The Hankel transforms are also applied to the corresponding shear and normal stresses, the force terms and the boundary and initial conditions as well.

To determine the radial and vertical components, it is necessary to solve the coupled system given by (7) and (8) using finite difference methods after which the spatial displacement components can be recovered through equation (5) and (6). The finite difference analogues to equation (7) and (8) given by (Ames, 1968) below are accurate to a second order in both space and time $O[(\Delta z)^2, (\Delta t)^2]$ and may be written as

$$\Phi_{i,j}^{m+1} = \left(\frac{\delta t^2}{\rho_{i,j}\delta s^2}\right)\left[a_{i+1,j}\Phi_{i+1,j}^{m} + a_{i,j}\Phi_{i-1,j}^{m} + b_{i,j+1}\Phi_{i,j+1}^{m} + b_{i,j}\Phi_{i,j-1}^{m}\right] - \Phi_{i,j}^{m-1}$$

$$\left[2 - \frac{n^2\pi^2\delta t^2}{c^2\rho_{i,j}}\lambda_{i,j} - \frac{\delta t^2}{\delta s^2 \rho_{i,j}}\left[\left(b_{i,j+1} + b_{i,j}\right) + \left(a_{i+1,j} + a_{i,j}\right)\right]\Phi_{i,j}^{m}, \tag{9}$$

where δs stands for the spatial sampling rates in the $(x,z) \longrightarrow (i,j)$ directions and δt stands for the time steps in the m direction. The quantities $a_{p,q}$ and $b_{p,q}$ are the density-normalized stiffness coefficients can be determined from derivation which appears in Daley (2010).

Number of terms in inverse transform series:

The number of terms required to approximate the infinite inverse series summation increases linearly with the value of a (the distance from the source to the perfectly reflecting boundary at radial distance). Equation 9 is solved for these values of n, ($0 \leq n \leq n_{max}$), where n_{max} is the number of terms in the finite inverse Hankel transform (3) and (4) required to approximate the inverse series summation (5) and (6) where $n = k_y a/\pi = 2fpa$, where p = horizontal slowness, f = bandlimited frequencies and a = pseudo-boundary distance from the source.

The stability criterion

Daley (2007) presented the stability condition for the coupled P-Sv wave problem of equation 7 and 8 as

$$\frac{(\Delta t)^2}{(\Delta z)^2}\left(V_{qp}^2 + V_{qS_v}^2\right) + \frac{(\Delta t)^2 {k_i}^2}{4}\left(V_{qp}^2 + V_{qS_v}^2\right) \leq 1, \tag{10.1}$$

$$\frac{(\Delta t)^2}{(\Delta z)^2}\left(V_{qp}^2 + V_{qS_v}^2\right) \leq 1, \tag{10.2}$$

where $V_{qp}^2 = \max(a_{11}, a_{33})$ is the maximum value that either a_{11} or a_{33} attains on the finite difference grid and $V_{qS_v}^2 = \max(a_{55})$, where the previous definitions hold. The value of k_i is the minimum non-zero value in the series $(k_i : i = 1, n)$ with n being the maximum number of roots used in the infinite series summation approximation.

Receiver-angle correction

The receiver-angle effect and the closely related surface-conversion effect are two of the effects that must be corrected for a 3-C dataset assuming that we wish to estimate the reflection coefficient. The receiver-angle effect occurs at the receiver when wave traveling upward from the earth's interior is incident at non-zero angle at the receiver. The displacement of this wave will be observed on both vertical and horizontal geophones at the interface. A complete understanding of the total displacement wavefield at the surface will consider all receiver effects including the receiver-emergence angle effect and the free surface effect at the receiver.

For a vertical geophone receiver, the receiver-angle correction for pure PP mode will be

$$\frac{1}{cos\theta_0} = \frac{incoming\ signal}{(vertical\ component\ of\ incoming\ signal)} \tag{11.1}$$

where θ_0 is the emergence angle at the receiver; thus, the actual amplitude A should be

$$A = \frac{1}{cos\theta_0} * recorded\ amplitude\ of\ vertical\ component, \quad (11.2)$$

we know that

$$\frac{sin\theta_0}{V_0} = \frac{sin\theta(z)}{V(z)} = p \text{ (Ray parameter)}$$

$$sin\theta_0 = V_0\left(\frac{sin\theta(z)}{V(z)}\right) = pV_0 \ , \quad (11.3)$$

$$cos\theta_0 = (1 - (sin\theta_0)^2)^{1/2} = (1 - (pV_0)^2)^{1/2} \ ,$$

The angle-of-emergence correction for a P-wave on the vertical component or an S-wave on a horizontal component is represented as

$$A_c(t,p) = \frac{A'}{cos\theta_0} \quad (11.4)$$

Where $A_c(t,p)$ is the corrected amplitude as function of time, t and ray-parameter p, A' is the original recorded amplitude. This correction varies with offset, time and velocity of the weathered layer. The receiver-angle correction, unlike the geometric-spreading depends greatly on near surface properties. A close related effect to the receiver-emergent angle effect is the free-surface effect, the correction for the free-surface effect is not trivial because the free surface is also contaminated by cumulative effects in the near surface e.g. interference.

Free-surface effect

This is as a result of backscattered waves occurring at the solid-air interface. The conversion generated depends on the incidence mode, on the elastic properties of the weathered layer at the free-surface and on the incidence angle at the free surface. The resultant wave movement is known as the free surface effect or the surface conversion effect. This effect can be expressed as vertical and horizontal displacements which are of considerable interest in exploration since these displacements correspond to the components of displacement of a Cartesian geophone deployed on the land surface.

The analysis of the free-surface response considering the 2-D case (horizontal and vertical response directions) and plane wave incidence assuming an isotropic homogeneous medium is shown below. An Incident P wave generates reflections of P wave and converted S wave. Similarly an incident S wave generates reflections of S waves and converted P waves. The two conditions to be satisfied are stress and displacement equilibrium, namely; (1). The displacement caused by the incidence wave is the result of the incident and the reflected wave displacements. (2). the resulting stresses at the free surface are zero.

Figures 1a and b illustrates the geometry and the terms for incident P- and S- wave arriving at the free surface.

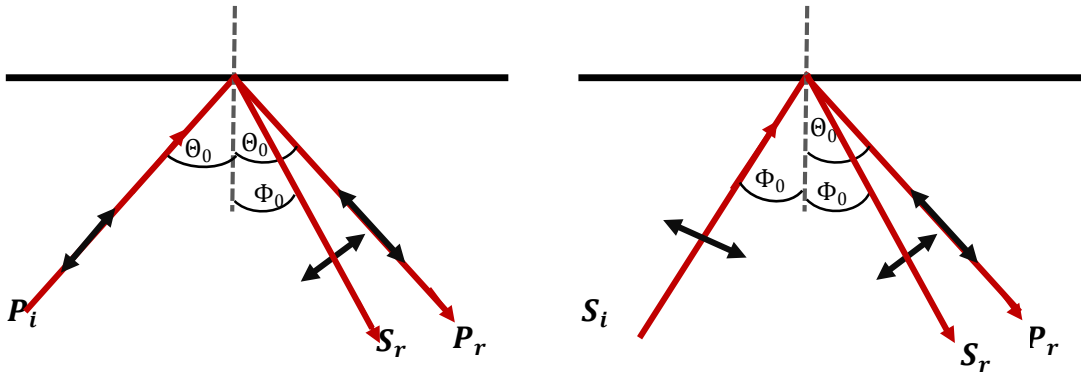

(a) Incident P-wave **(b) Incident S-wave**

Fig 1: Free-surface event response in the case of (a) incident P-wave and (b) incident S-wave. Each one of them generates converted waves of the other type.

For the case of an incident P-wave (Figure 1a); the total wavefield recorded by a vertical and horizontal geophone can be expressed as:

$$G_z = P_I cos\Theta_0 + R_{pp} P_I cos\Theta_0 + R_{ps} P_I sin\Phi_0 \quad (12.1)$$

and

$$G_r = P_I sin\Theta_0 + R_{pp} P_I sin\Theta_0 + R_{ps} P_I cos\Phi_0 \quad (12.2)$$

For the case of an incident S-wave (Figure 1b); the total wavefield recorded by a vertical and horizontal geophone also can be expressed as:

$$G_z = S_I sin\Phi_0 + R_{ss} S_I sin\Phi_0 + R_{sp} S_I cos\Theta_0 \quad (12.3)$$

and

$$G_r = S_I cos\Phi_0 + R_{ss} S_I cos\Phi_0 + R_{sp} S_I sin\Theta_0 \,, \quad (12.4)$$

where P_I and S_I = incidence P- and S-wave. R_{pp} ,R_{ps}, R_{ss} and R_{sp} are the reflection coefficients at the free surface; Θ_0 and Φ_0 are the incidence angles of P- and S-wave; G_z and G_r are the total vertical and horizontal wavefields recorded by a vertical and horizontal geophone.

Dankbaar (1985) gives the mathematical expressions for the relative amplitudes as a function of the angle of incidence and the elastic parameters for the expected horizontal and vertical component receiver measurements assuming an incident P or SV wave on a

free surface. These expressions are a particular case of the Zoeppritz equations (without a transmission medium). For an incident P-wave, Dankbaar's expression leads to the relationship between the displacement angle ϕ and the incidence angle θ given below as

For P waves; $\tan\phi = \frac{2sin\theta\sqrt{r^2-sin^2\theta}}{r^2-2sin^2\theta}$ (13a)

For S-wave; $\tan\phi = \frac{r(1-2sin^2\theta)}{2sin\theta\sqrt{r^2-sin^2\theta}}$ (13b)

Where $r = {V_p}/{V_s}$

METHOD

We carried out synthetic computation of elastic waves for an isotropic media using the AMM method and conducted several numerical analyses to correct for spherical divergence, surface effects at the receivers and wavelet effect in order to estimate reflection coefficients from the synthetic data. After the wavefields have been computed, we used either the raytraced traveltimes or we manually picked the P-P reflection events and the converted PS reflection events graphically depending on the trajectory of the reflected events at longer offsets. Each pick is adjusted to the nearest maximum peak within a fairway using a picker tool. In some cases where the amplitudes do not define a specific AVO/AVA behavior, we smooth the picks and model with a low order polynomial. In other cases, only smoothing is necessary, and no need for polynomial fitting. The graphically picked traveltimes are also fitted with a second-order polynomial in offset. The ray parameters were computed using two methods; (1) from the raytracing and (2) from the slope (time dip) of the graphically picked times. The amplitudes are corrected for geometric spreading, receiver-emergence angle effect and for surface conversion at the free surface. The "pfreesurf" and "freesurf" codes which follows after equations 12.1, 12.4 and 13 are used to compute the free surface coefficients for emergent P- and emergent S- waves for data whose receivers are at the free surface.

RESULTS

The results that ensued from previous sections are discussed here. We used the AMM method to compute synthetic seismogram (figure 4) for an explosive point source and an isotropic media modelled from the CREWES 0808 well log shown in figure 2. The model is 4km long with receiver spacing at every 0.005 km. The first reflector is 1.36km deep and the source is placed at the first receiver. The traveltimes of these results are compared in figures 5 to 8 with the predicted two-way traveltimes results from ray theory. Also for amplitude comparison for AVO and AVA analysis, the AMM amplitudes are compared with the exact Zoeppritz equation. Figures 9 to 12 shows the amplitude variation with angle and with offsets from the first reflector. Figure 12 also show the effect of free-surface on amplitude values for two case acquisition scenarios; acquisition with receivers at or close to the free-surface and for buried receivers.

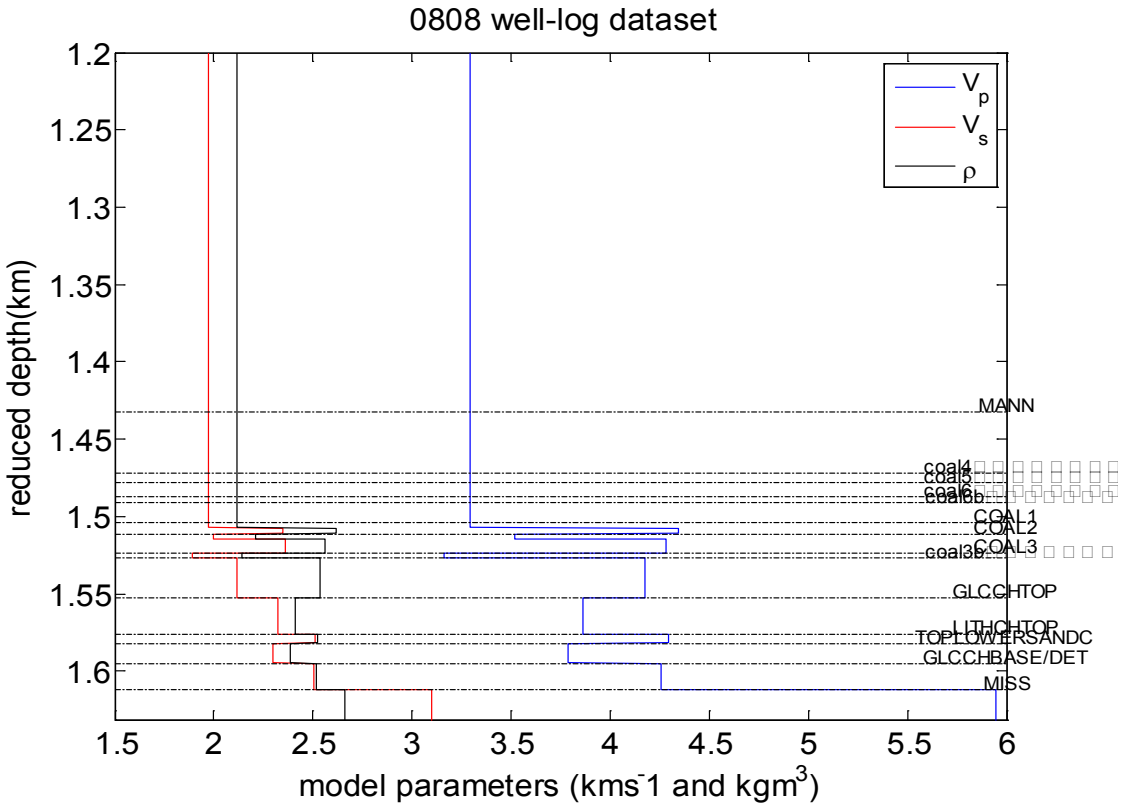

Fig 2: Wireline data used to generate 2D model parameters for theoretical seismogram computation. There are 21 defined formations tops with layers block by the distinct thicknesses of each of the marked tops. The picked amplitudes are from reflections from the top of Mann formation.

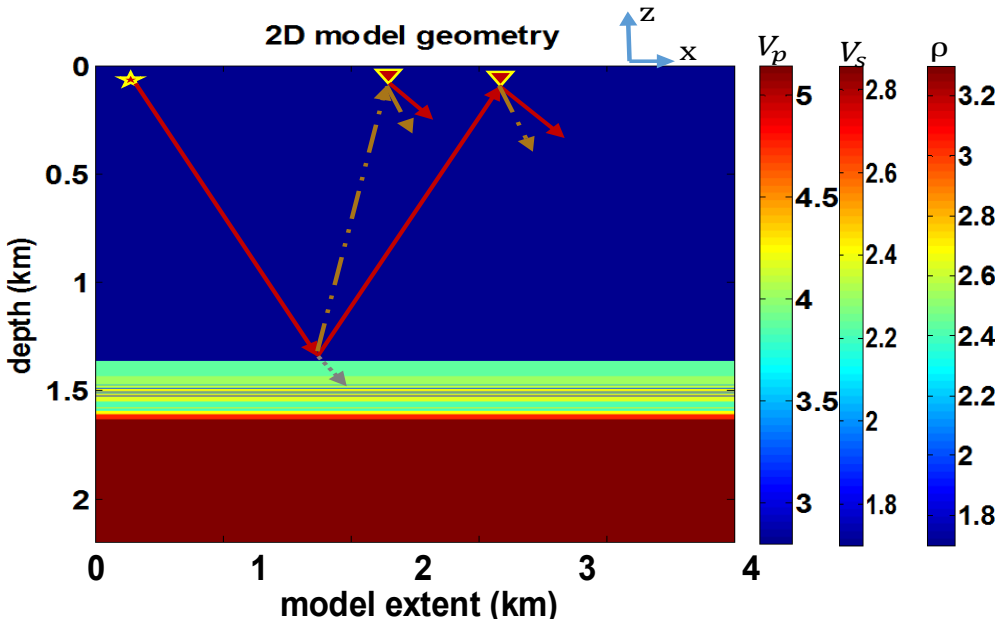

Fig 3. 2 D model geometry with 21 defined layers and showing a cartoon of P-Sv wave raypaths from the first impedance contrast highlighting geophone response at the receiver and surface conversions. The red arrows denote a P-wave raypath, the yellow arrow denote an S-wave ray-

path. The colorbars represents the P-wave velocity, Shear wave velocity and density values at depth obtained from the sonic, dipole-sonic and bulk density log measurements from the 0808 wireline dataset.

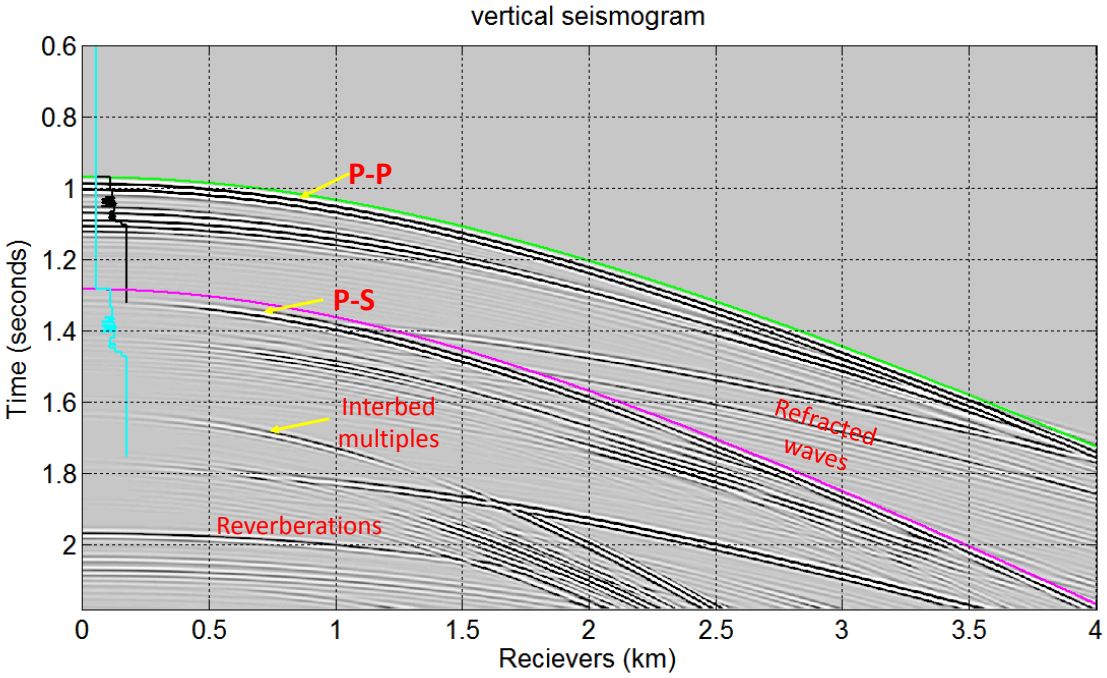

Fig. 4a. Time-domain shot-gather for total vertical wavefield recorded by the vertical geophones showing reflected events as well as refracted, converted waves and multiples. The black and cyan logs are the zero offset PP and PS two-way traveltime-velocity function.

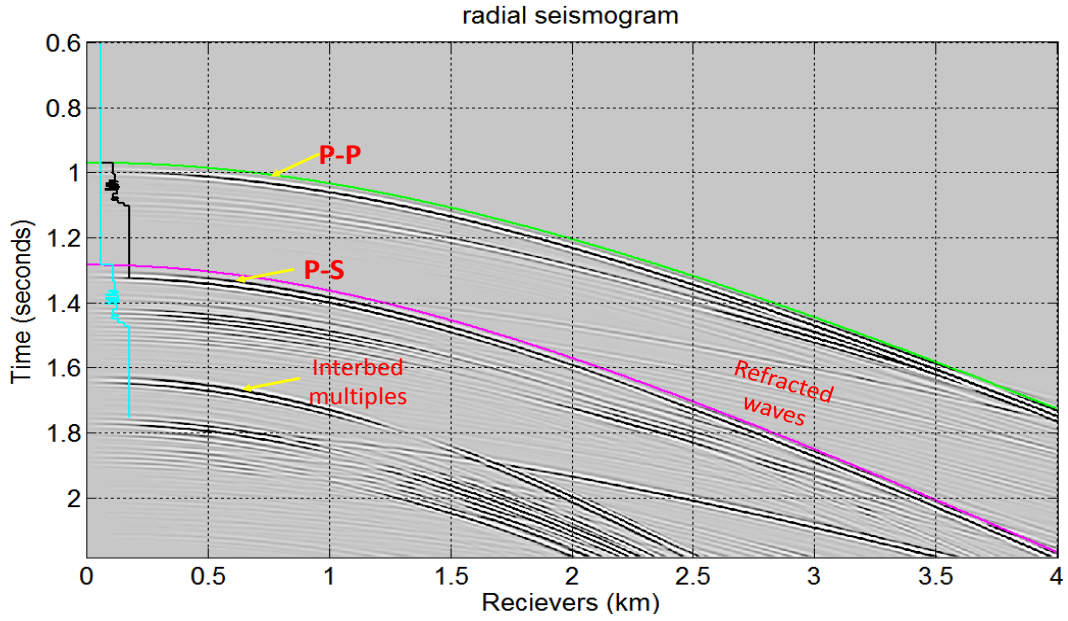

Fig. 4b. Time-domain shot-gather for total horizontal wavefield recorded by horizontal geophones. Other wave modes along with P- and converted PS-waves recorded are highlighted in magenta. Converted P-Sv wave amplitude are increases from for increasing non-zero offsets. Converted waves amplitudes are dimmed in both components, around 1.4 km and 2.3 km due to interference from S-refraction. The black and cyan logs are the zero offset two-way traveltime-velocity function.

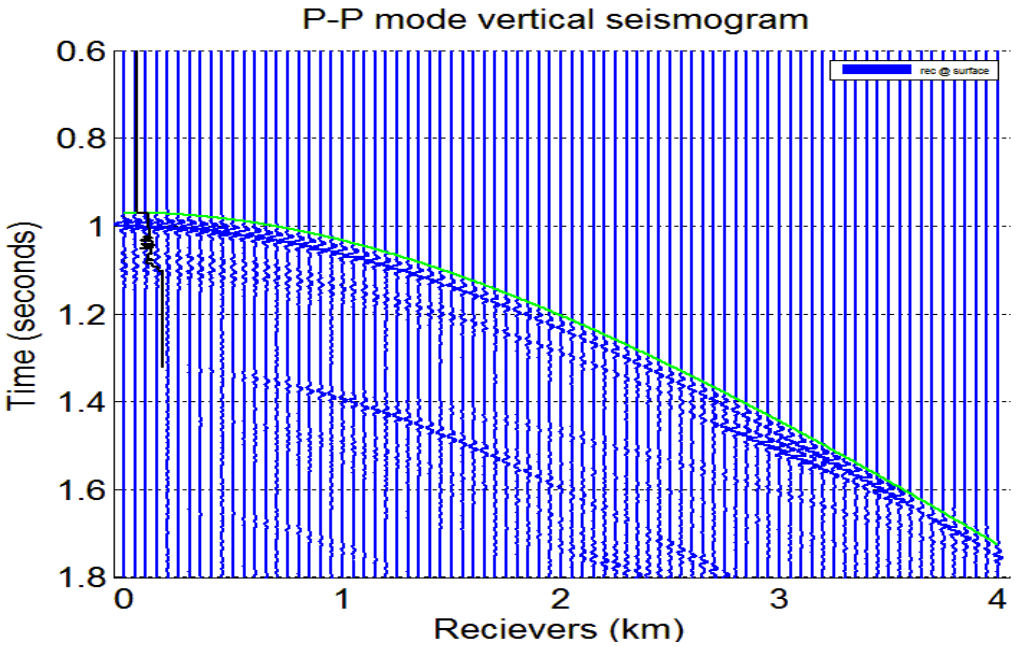

Fig 5. P-P reflections of vertical seismogram from the Alekseev-Mikhailenko Method (blue traces) matched with computed traveltimes from Ray theory (green curve) for first reflector. The black log is the zero offset two-way traveltimes. The computed travel times from AMM match well with the predicted arrival time of each reflection from Ray theory with little and unnoticeable deviation at very far offset.

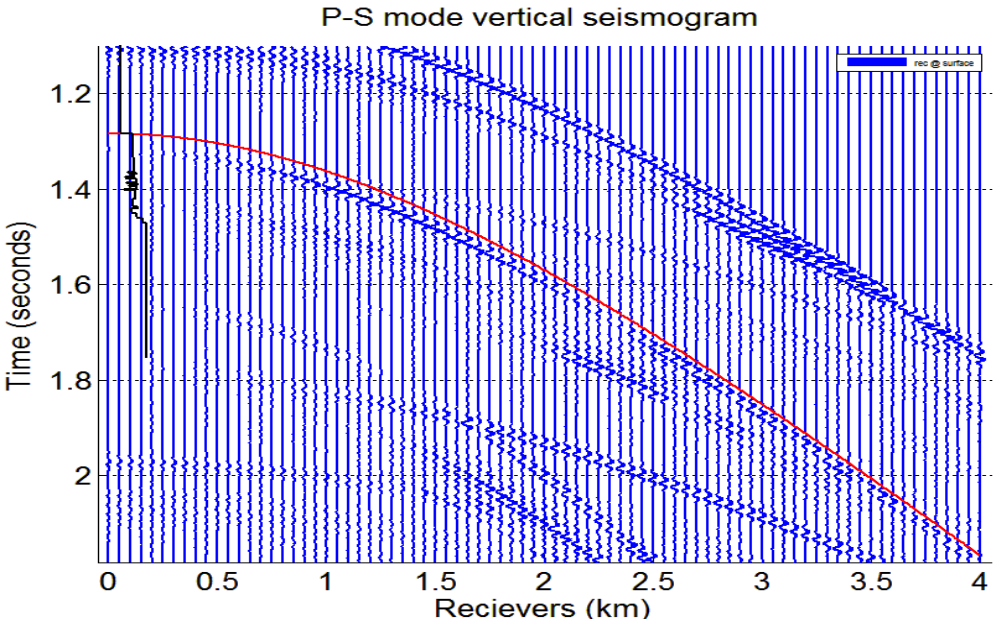

Fig 6. P-S reflections of vertical seismogram from the Alekseev-Mikhailenko Method (blue traces) matched with computed traveltimes from ray theory (red curve). The amplitudes at near offset is as expected for converted PS mode. The black curve is the interval velocity-time fu zero offset two-way traveltime-velocity function.

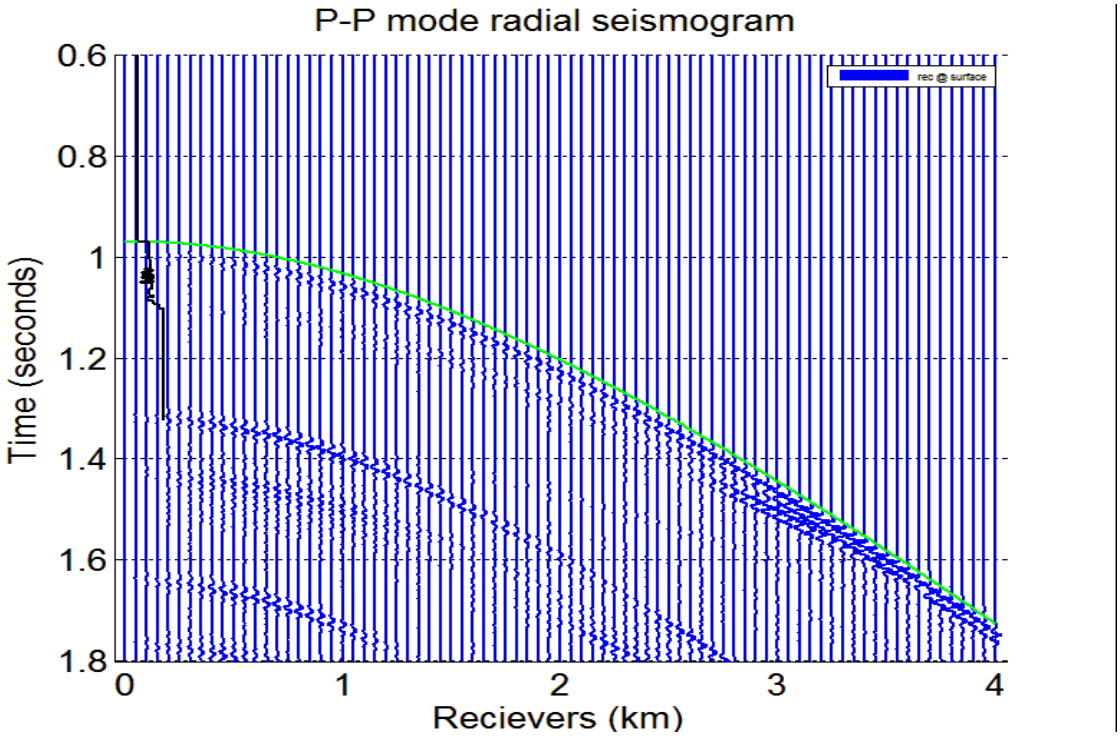

Fig 7. Recorded P-P mode on horizontal seismogram from the Alekseev-Mikhailenko Method (blue traces) matched with computed traveltimes from Ray theory (red curve). The black curve is the zero offset two-way traveltime-velocity function.

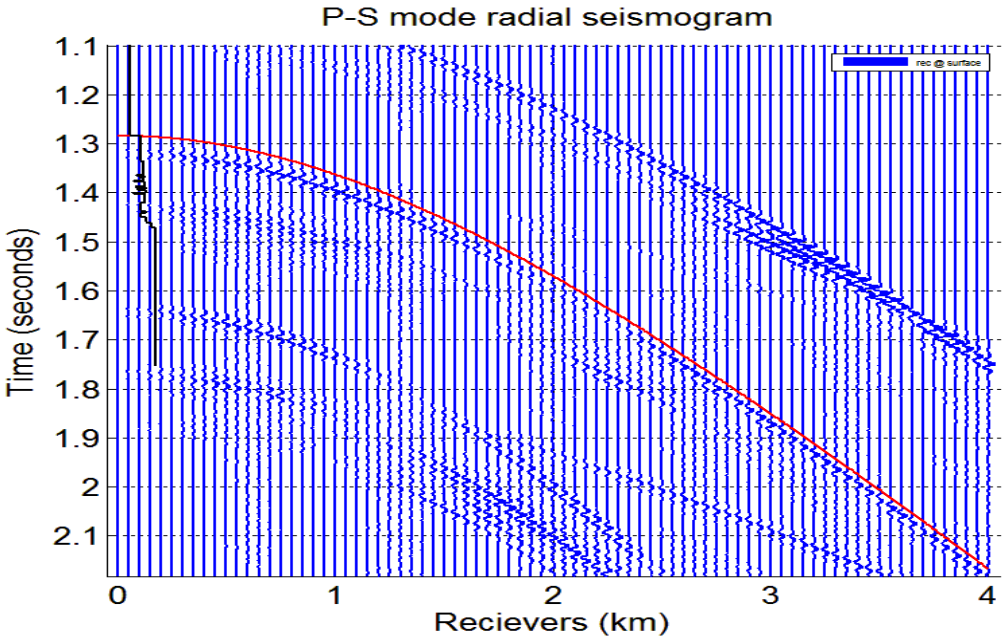

Fig 8. Converted P-S mode recorded on horizontal seismogram from the Alekseev-Mikhailenko Method (blue traces) matched with computed traveltimes from Ray theory (red curve). The traveltimes computation match the traced rays from ray-theory. The black log is the zero offset two-way traveltimes.

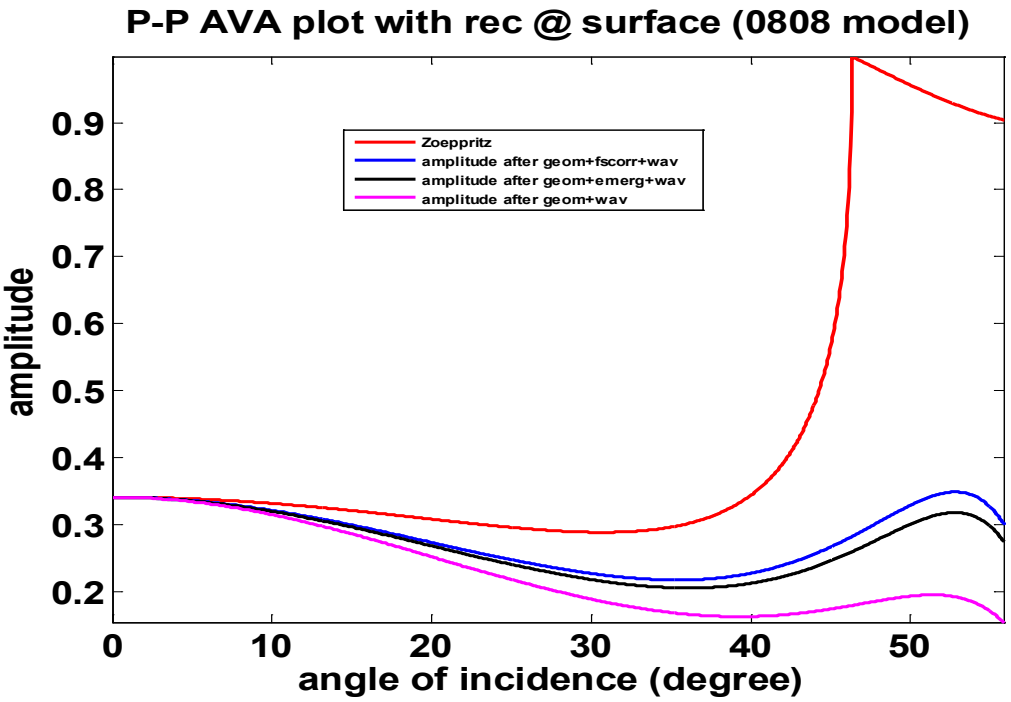

Fig 9a: P-P AVA amplitude plots before and after free-surface correction and emergence-angle correction when receivers are at the free surface.

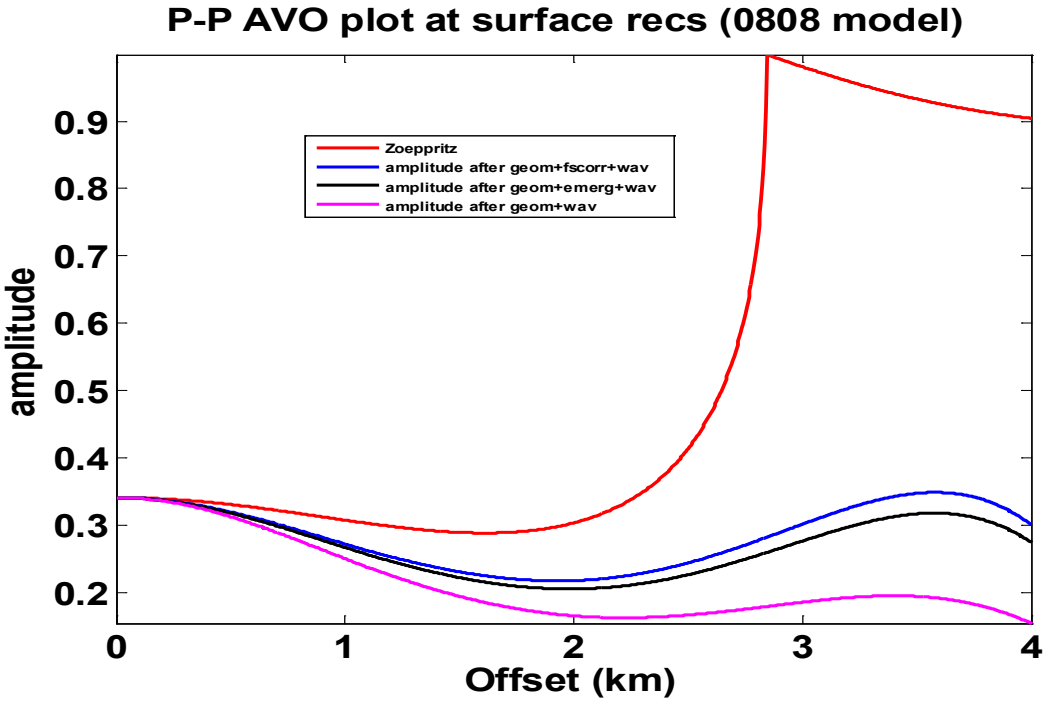

Fig 9b: P-P AVO amplitude plot before and after free-surface correction and emergence-angle correction when receivers are at the free surface. Zoeppritz amplitude matched the AMM computed amplitude at near incidence angles up to 10 degrees. Amplitude trends are similar at pre-critical angles (Critical angle is at 46.2^0). Post-critical reflections changes gradually for AMM.

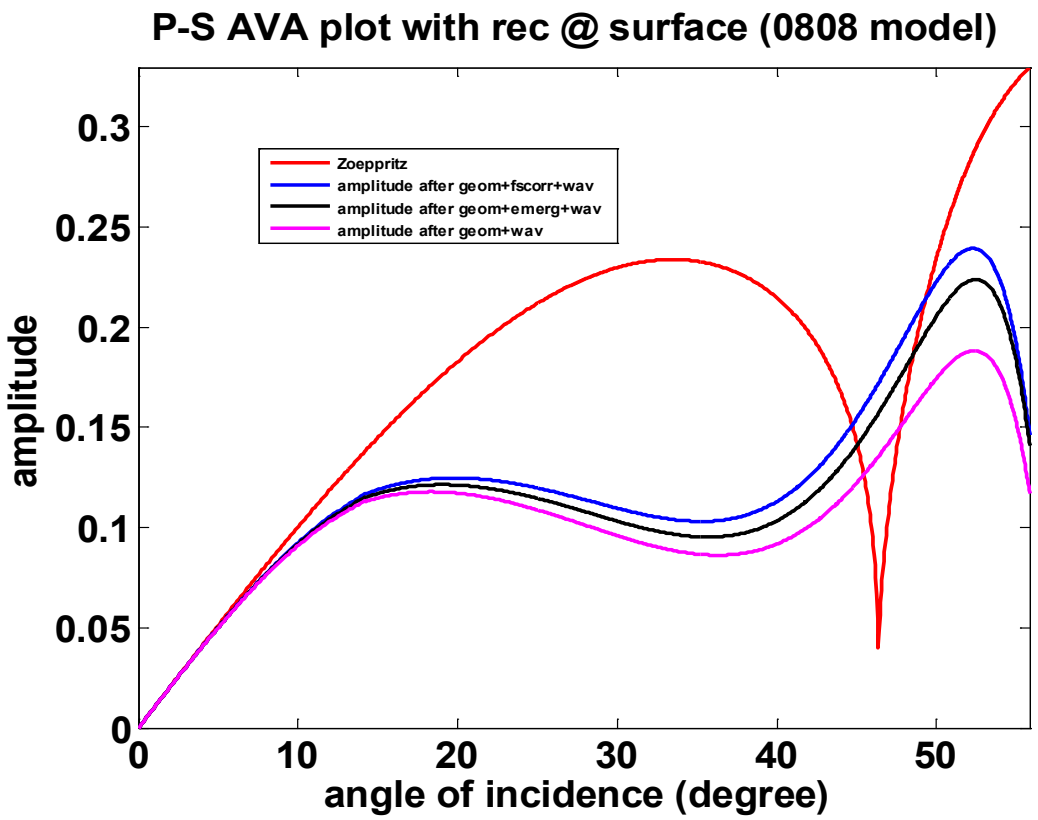

Fig 10. Converted PS mode AVA amplitude plots before and after free surface and emergence-angle correction for a scenario where receiver is on the free surface. The amplitudes of the converted wave deviates from the plane wave Zoeppritz equation at above 10 degrees.

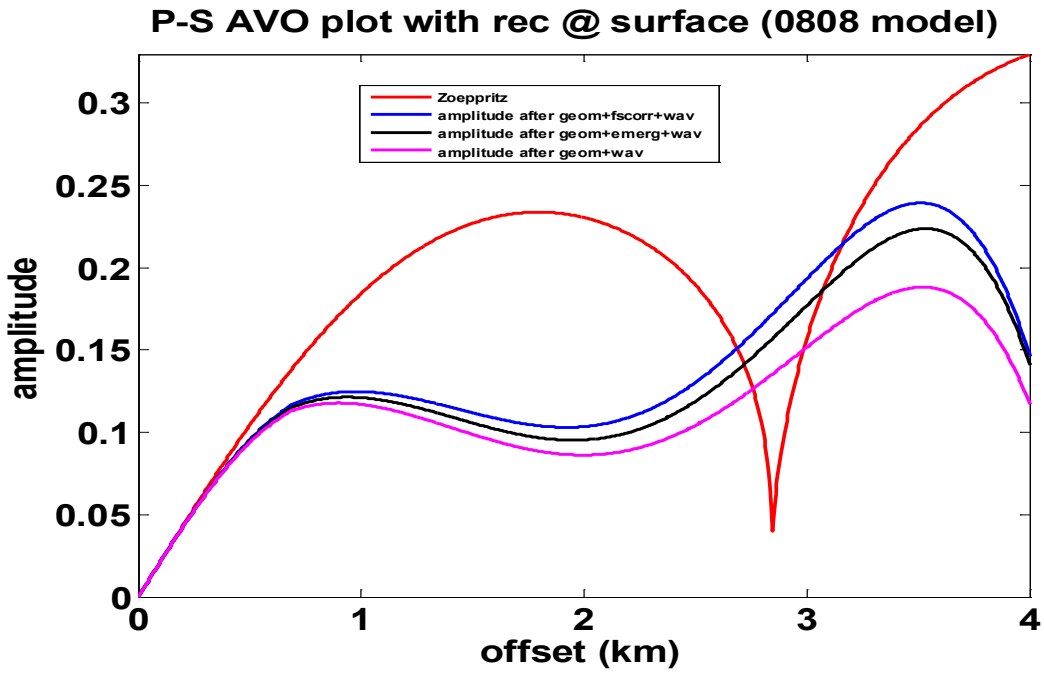

Fig 10b. Converted PS mode AVO amplitude plots before and after free surface and emergence-angle correction for a scenario where receiver is on the free surface. At near vertical incidence,

both amplitudes matched up to about 0.5 km. The converted wave amplitudes deviates from Zoeppritz equation at above 500m source-receiver offset.

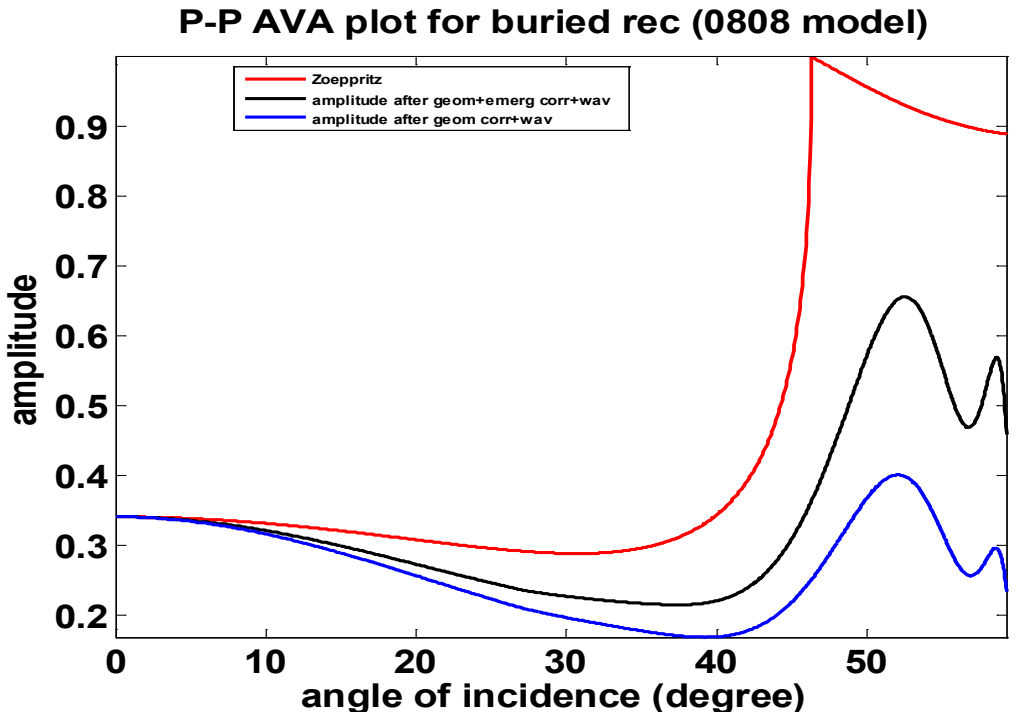

Fig 11a: P-P AVA amplitude plot before and emergence-angle correction for buried receivers.

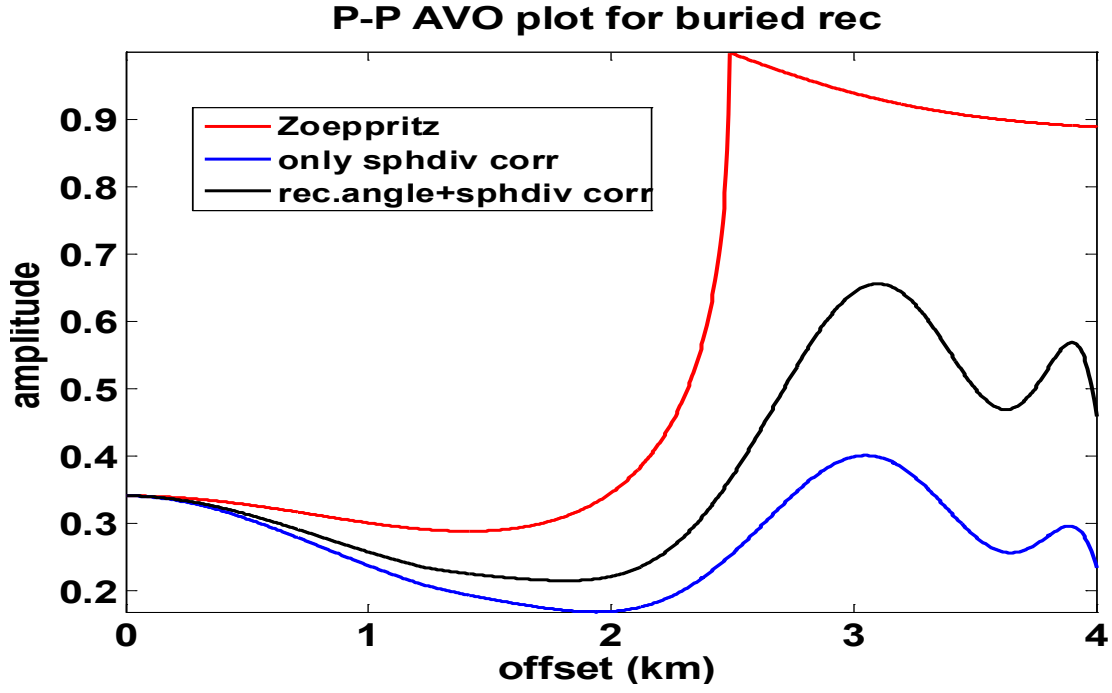

Fig 11b: P-P AVO amplitude plot before and emergence-angle correction for buried receivers.

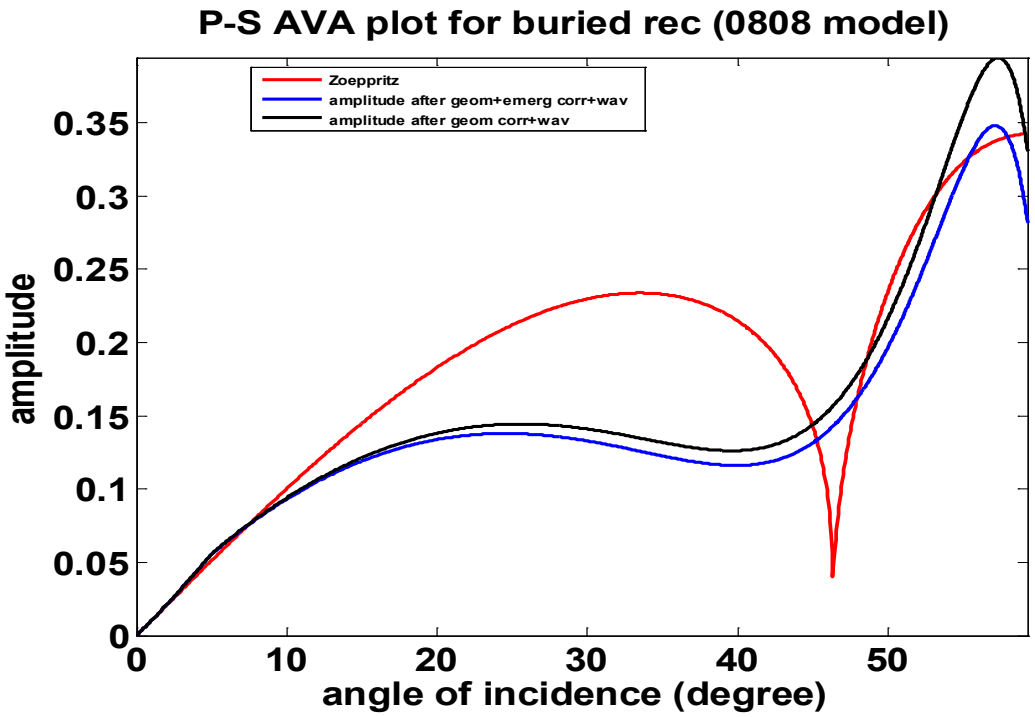

Fig 12a: P-S AVA amplitude plot before and emergence-angle correction for buried receivers. . No free surface correction was applied because the receivers are buried. We see that at near-vertical incidence, the blue and black curves denoting the AMM corrected amplitudes have about the same amplitudes with the Zoeppritz amplitudes and deviate at longer angles.

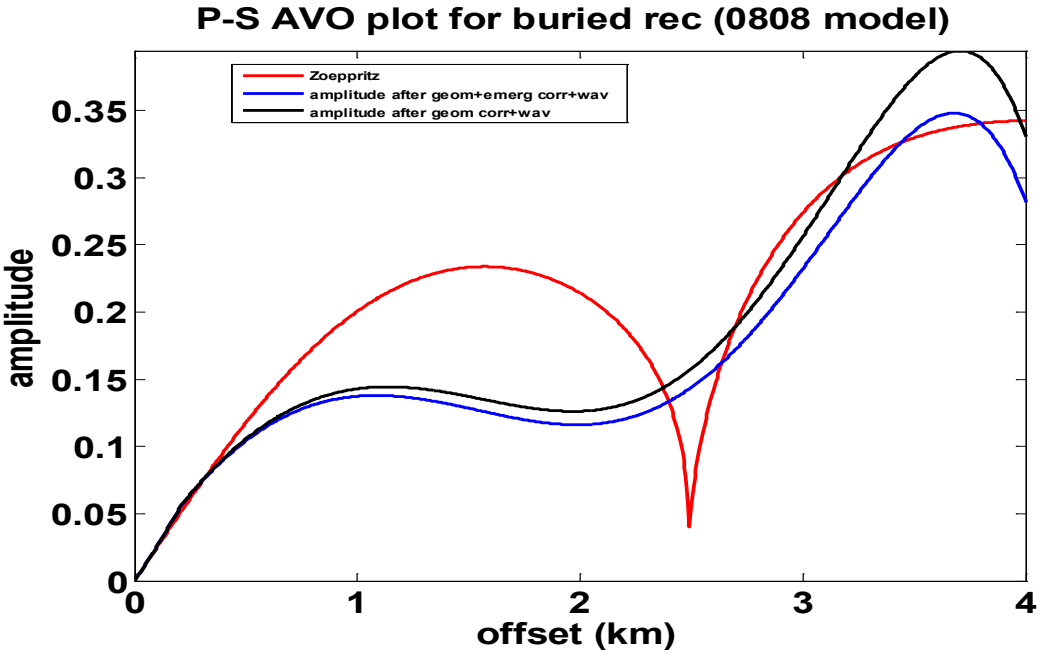

Fig 12b: P-S AVO amplitude plot before and emergence-angle correction for buried receivers. No free surface correction was applied.

A close comparison of free surface effect on total P-P amplitude shown in figure 9 to figure 12 shows the significance of applying free surface correction to surface receivers or burying the

receivers at depths where free-surface reflections can be comfortably avoided. It is important to note that all amplitudes have been corrected for spherical divergence, wavelet effect and emergence-angle effect. The free surface is more significant at long offset.

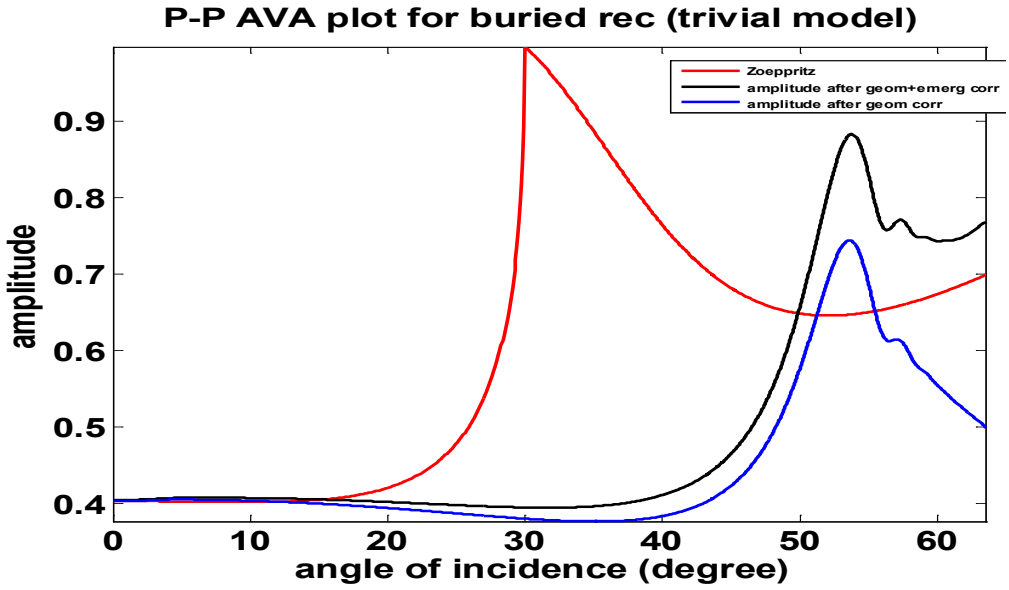

Fig 13: P-P AVA amplitude plot before and emergence-angle correction for buried receivers.

Figure 13 is the P-P AVA plot for a longer offset, larger angles, a trivial one layer model with a reflector at 1.5 km and maximum source receiver offset of 5km. The computed amplitudes matched the Zoeppritz amplitudes up to the plane-wave critical incidence which is at 30 degrees.

CONCLUSION

The solution of coupled P-Sv wave propagation in a radially symmetric vertically inhomogeneous media as well as the solution to correct for spherical divergence, receiver-angle effect and wavelet effects for receivers at the free-surface and for buried receivers have been presented. We have also extended this study to consider free-surface effects supposing isotropic homogenous overburden. The results presented here show that AMM gave exact solution to the elastic wave problem, it is practically implementable. After correcting for emergence-angle and free-surface conversion effect at the receiver, the P-P and P-S amplitudes match the plane wave Zoeppritz amplitude up to 10 degrees. The P-P amplitudes trend follows the same pattern with the plane wave Zoeppritz amplitudes with variance only in scale; the converted wave amplitudes however, but deviated from Zoeppritz from intermediate angles to far offset (angles). We infer that AMM can provide a good advantage for computing elastic wavefields for multicomponent processing and a good forward modeling kernel for an inversion algorithm.

Future work will include estimating anisotropy form the Bluebell-Altamont VSP dataset and using the AMM modeling algorithm to model VSP seismic response and incorporating this two workflow into an inversion scheme.

ACKNOWLEDGEMENT

We thank the sponsors of CREWES for their support. We also gratefully acknowledge support from NSERC (Natural Science and Engineering Research Council of Canada) through the grant CRDPJ 379744-08.

REFERENCES

Aki, K., and Richards, G. 1980. Quantitative seismology: theory and methods.

Alekseev, A.S., and Mikhailenko, B.G. 1980. Solution of dynamic problems of elastic wave propagation in inhomogeneous medium by a combination of partial separation in variables and finite difference methods. Journal of Geophysics, **48**: 161–172.

Ames, W.F. 1969. Numerical Methods for Partial Differential Equations. Barnes & Noble, New York, N.Y.

Daley, P.F., 2007, A hybrid method applied to a 2.5D scalar wave equation, CREWES Research Report, **19.**

Daley, P.F., Krebes, E.S., and Lines, L.R., 2008, a hybrid method applied to a 2.5D scalar wave equation. Canadian Journal of Earth Sciences, **45**: 1517–1525.

Daley, P.F., 2010, P-SV wave propagation in a radially symmetric vertically inhomogeneous TI medium: Finite difference hybrid method. CREWES Report, **22**.

Daley, P., F., and Margrave, G. F., 2012, Reflectivity modelling by finite difference. CREWES Research Report, **24**.

Dankbaar, J.W.M., 1985, Separation of P and S waves, Geophysical Prospecting, **33**, 970-986.

Martynov, V.N. and Mikhailenko, B.G., 1984, Numerical modelling of propagation of elastic waves in anisotropic inhomogeneous media for the half-space and the sphere, Geophysical Journal of the Royal Astronomical Society, **76**, 53-63.

Mikhailenko, B. G., 1984. Synthetic seismograms for complex three-dimensional geometries using an analytical-numerical algorithm. Geophysical Journal of the Royal Astronomical Society, **79**: 963 -986.

Muller, G., 1985. The reflectivity method: a tutorial, Journal of Geophysics, **58**: 153-174

Pascoe, L.J. Hron. F. and Daley. P., F., 1988. The Alekseev- Mikhailenko method applied to P- Sv wave propagation in an elastic medium. Canadian Journal of Earth Sciences, **25**. 266-234.